Nano Research 2018, 11(2): 1038–1056
https://doi.org/10.1007/s12274-017-1719-8
Research Article

ISSN 1998-0124
CN 11-5974/O4

Ultrasound-triggered release of sinoporphyrin sodium from liposome-microbubble complexes and its enhanced sonodynamic toxicity in breast cancer

Yixiang Li, Huanxiao An, Xiaobing Wang, Pan Wang (✉), Fei Qu, Yan Jiao, Kun Zhang, and Quanhong Liu (✉)

Ministry of Education Key Laboratory of Medicinal Resources and Natural Pharmaceutical Chemistry, National Engineering Laboratory for Resource Developing of Endangered Chinese Crude Drugs in Northwest of China, College of Life Sciences, Shaanxi Normal University, Xi'an 710119, China

Received: 15 April 2017
Revised: 3 June 2017
Accepted: 11 June 2017

© Tsinghua University Press and Springer-Verlag GmbH Germany 2017

KEYWORDS
ultrasound,
microbubble,
sinoporphyrin sodium,
sonodynamic therapy

ABSTRACT

Applying ultrasound (US) to drug delivery and disease therapy is important work. Sonodynamic therapy (SDT)—a comprehensive therapy using US and a sonosensitizer—exhibits antineoplastic activity in many tumors. In this study, we investigated the feasibility of using a new sonosensitizer (sinoporphyrin sodium, DVDMS) loaded into liposome–microbubble complexes (DLMBs) as a possible candidate to enhance SDT against breast cancer. DLMBs were synthesized via the biotin–avidin linkage and confirmed to have good US response. US-induced cavitation played a key role to trigger a boosted payload release from DLMBs and improve the cellular uptake and intratumoral diffusion of DVDMS to realize better SDT effect. The combination of DLMBs and US treatment resulted in significant changes to cell morphology, mitochondria damage, and cell apoptosis *in vitro*. *In vivo*, the combined treatment markedly inhibited tumor growth, which appeared to result from increased apoptosis and reduced proliferation activity. The significant increase in the antitumor effect of DLMBs plus US suggests their potential use as a new approach to promote the killing activity of SDT against breast cancer.

1 Introduction

Although ultrasound (US) imaging is a well-established diagnostic technique, its potential in therapeutics has also been explored for several decades [1–3]. Sonodynamic therapy (SDT) is a form of ultrasonic therapy in which specialized agents known as sonosensitizers are administered to increase the extent of preferential damage exerted by US against tumor cells [4, 5]. Preliminary studies examining the antineoplastic mechanism of SDT have indicated that US activates reactive oxygen species (ROS) generation in the presence of sonosensitizers to elicit oxidative stress, which plays a key role in apoptosis induction in

Address correspondence to Pan Wang, wangpan@snnu.edu.cn; Quanhong Liu, lshaof@snnu.edu.cn

tumor cells [4–10]. To date, SDT has shown promise as a potentially vital alternative to traditional treatment modalities and has yielded impressive anticancer effects in both *in vitro* and *in vivo* studies [6–8]. Moreover, some articles about the clinical trials of SDT have indicated that it is well tolerated and has a significant therapeutic effect in advanced breast cancer [8, 11].

With the development of SDT, some adjuvant agents were introduced to enhance its sonodynamic effects [12, 13]. In 2015, Wang et al. reported that SonoVue® microbubbles (MBs) significantly enhanced the antitumor effects of SDT [14]. Several other studies also came to the same conclusion [15, 16]. MBs—small gas-filled microspheres ranging from 1–10 μm in diameter—can provide nuclei for the initiation of cavitation. When exposed to US, MBs passing through the beam interact with the acoustical energy. The expansion, contraction, and violent collapse of MBs in response to US can create microstreaming, high-velocity jets, and shock waves. Additionally, MBs increase the absorption of sonic energy through cavitation, thus improving the penetration of US into tissues [17, 18]. Acoustic cavitation can affect neighboring cells by either stimulating endocytosis or by the formation of temporary pores in the cell membranes (known as sonoporation), to facilitate macromolecules to be transported into the targeted cells [19–21]. Therefore, when US, MBs, and sonosensitizers act together, the antitumor efficacy of SDT would be greatly improved.

Over the years, MBs have gained popularity as contrast agents for US imaging. In addition to their clinical applications, MBs are under preclinical investigation as potential drug- and gene-delivery carriers. Therapeutic agents are co-administrated with MBs in several ways; drugs can be co-injected with the MBs, encapsulated in the shell/lumen, covalently linked at the shell surface, or encapsulated in nanoparticles and then linked with the MBs [20, 22, 23]. Liposome–MB complexes developed by Kheirolomoom et al. are a promising system to realize US-mediated drug delivery and improve therapeutic efficacy [24]. In this system, the liposomes encapsulate drugs and covalently link at the MBs' surface. This kind of carrier is considered to load more drugs on the MBs than the other loading strategies do [24, 25]. US triggers the burst release of payloads from the carrier, through destruction of its lipid shell via a controlled release mechanism, and simultaneously transiently perforates the plasma membrane of cells through sonoporation, leading to enhanced trans-membrane transport of therapeutic agents into cells and facilitating the therapeutic outcome [25–27]. Herein, we speculated that if a sonosensitizer was encapsulated in a liposome and linked to an MB, it would be acoustical-controlled released and activated to produce cytotoxic free-radical substances, gaining much better sono-cytotoxic effects on tumors.

Sinoporphyrin sodium (also called DVDMS)—a novel photo-/sono-sensitizer depurated from photofrin II by Prof. Fang et al. at the Chinese Academy of Medical Sciences—has been approved for pre-clinical trials in China [28]. DVDMS is a hydrosoluble sensitizer with a strong absorption coefficient and high ROS yield. DVDMS has the characteristics of spontaneous fluorescence (the excitation wavelength is 408 nm; the emission wavelength is 626 nm). Previous studies have confirmed that DVDMS is an excellent porphyrin sensitizer with great potential in therapy and imaging applications. Wang et al. have indicated that the cytotoxicity of DVDMS combined with light is much stronger than that of photofrin II against tumors [29]. Additionally, Yan et al. reported that DVDMS-loaded polyethylene glycol (PEG) modified graphene oxide is a great contrast material for enhanced optical imaging and fluorescence/photoacoustic dual-modal imaging; it also improved the effects of photodynamic therapy (PDT) and photothermal therapy (PTT) [30, 31]. Moreover, our preliminary studies have confirmed that DVDMS possesses good sono-cytotoxicity against several tumors [14, 32, 33]. In this study, to determine a method to enhance the antineoplastic effect of DVDMS-SDT, we designed and validated a US-responsive platform based on DVDMS-loaded liposome-MB complexes (DLMBs). The efficacy of US-triggered DVDMS release from the DLMBs and its sonodynamic toxicity on breast cancer were determined both *in vitro* and *in vivo*.

2 Experimental

2.1 Materials

1,2-Dipalmitoyl-sn-glycero-3-phosphocholine (DPPC),

1,2-distearoyl-sn-glycero-3-phosphoethanolamine-N-methoxy(polyethylene-glycol)-2000 (DSPE-mPEG 2000), DSPE-PEG 2000–biotin, and cholesterol were purchased from Avanti Polar Lipids Inc. (Alabaster, AL, USA). 3-(4,5-Dimethylthiazol-2-yl)-2,5-diphenyltetrazolium bromide (MTT), 6-amino-9-(2-methoxycarbonylphenyl) xanthen-3-ylidene]azanium chloride (rhodamine), 2,7-dichlorodihydrofluorescein diacetate (DCFH-DA), 4′,6-diamidino-2-phenylindole (DAPI), and fluorescein isothiocyanate-dextran 500 KD (FD 500) were purchased from Sigma–Aldrich (St. Louis, MO, USA). An Annexin V-FITC Apoptosis Detection Kit was obtained from Keygen Technology Co. Ltd. (Nanjing, Jiangsu, China). All other reagents were commercial products of analytical grade.

DVDMS (molecular formula: $C_{68}H_{66}N_8O_9Na_4$, molecular weight: 1,230.265 Da, purity: > 98%) was the property of Qinglong Hi-tech Co. Ltd. (Jiangxi, China) and was kindly provided by Prof. Qicheng Fang from the Chinese Academy of Medical Sciences (Beijing, China). DVDMS was dissolved in phosphate-buffered saline (PBS) to a stock concentration of 4 mg/mL and stored in the dark at −20 ℃.

2.2 Cell culture and animal model

Human breast cancer MDA-MB-231 cells and mouse breast cancer 4T1 cells were obtained from the Cell Resource Center of the Chinese Academy of Science, China. Both cell types were cultured in Dulbecco's modified Eagle's medium (DMEM, Gibco, Life Technologies, NY, USA) supplemented with 10% (v/v) fetal bovine serum (Life Technologies, CA, USA), 100 U/mL penicillin-streptomycin solution (Hyclone, UT, USA), and 1 mM L-glutamine (Sigma-Aldrich, St. Louis, MO, USA) at 37 ℃ in a humidified atmosphere of 5% CO_2. Cells in the exponential growth phase with a viability of ≥ 98%, determined by the trypan blue exclusion test, were used for this study.

BALB/c mice (female) were supplied by the Animal Resource Center of the Fourth Military Medical University (Xi'an, China). The mice were housed at room temperature with a 12 h light/dark cycle and allowed free access to food and water. After a 1-week acclimation period, the mice were subcutaneously injected in their left oxter with 1×10^6 4T1 cells. When the tumors grew to about 5 mm in diameter, the mice were ready for experimentation. The animal experiments were performed in accordance with the National Institute of Health's Guide for the Care and Use of Laboratory Animals and were approved by the Institutional Animal Care and Use Committee of Shaanxi Normal University (Xi'an, Shaanxi, China).

2.3 Ultrasound apparatus

The ultrasonic device was the same as that described in previous studies (Scheme 1) [14, 34]. A cell-based therapeutic pulsed ultrasound apparatus (Sheng Xiang High Technology Co. Ltd., Shenzhen, Guangdong, China) was applied for *in vitro* experiments in this study. For *in vitro* cell experiments, the ultrasonic parameters were set as follows: frequency of 1 MHz, intensity of 0.4 W/cm^2, duty cycle of 30%, and duration of 90 s. For *in vivo* experiments, a home-made focused US transducer was used to treat tumor-bearing mice. Under anesthesia with pentobarbital, tumor-bearing mice were placed facing downwards directly at the focal point for sonication with load power of 3 W and frequency of 1 MHz for 3 min.

2.4 Preparation of DLMBs

2.4.1 *Preparation of DVDMS liposome-biotin*

The DVDMS liposome-biotin (DL-biotin) complex was prepared by the filming-rehydration method. Briefly,

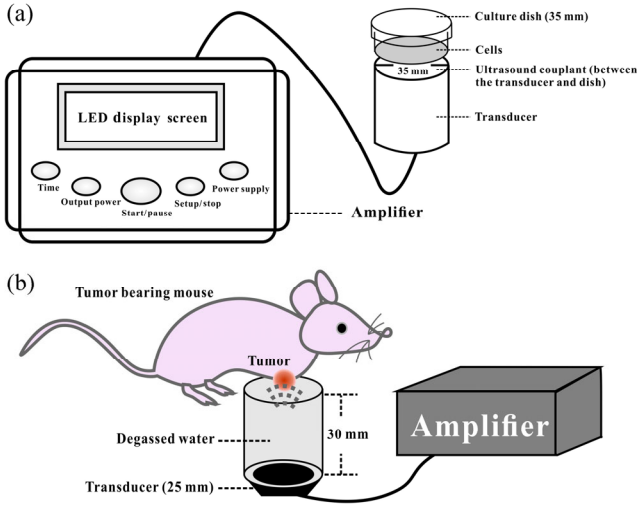

Scheme 1 Schematic diagrams of the ultrasound setups. (a) Cell-based therapeutic pulsed US apparatus for *in vitro* experiments. (b) Home-made focused US device for treating xenografts in tumor-bearing mice.

appropriate amounts of DPPC, cholesterol, and DSPE-PEG 2000–biotin (molar ratio of 67:23:10) were dissolved in chloroform in a round-bottom flask, and then the solvent was removed through vacuum evaporation under reduced pressure for 2 h. The thin dried phospholipid blends were hydrated at 60 ˚C with a buffer consisting of PBS (0.01 M, pH 7.2; 4 mg/mL of final lipid concentration) and DVDMS (the ratio of DVDMS and lipids was 1:40, w/w). The mixture was shaken and then sonicated (40 kHz) for 37 min in a water bath. This preparation was subjected to high-intensity probe sonication (20% amplitude) for 50 s to produce small unilamellar vesicles. After standing for 10 min, the encapsulated free DVDMS were passed through a Sephadex column (Sephadex G-50, Sigma-Aldrich) equilibrated with PBS. The final liposomes were stored in tight containers at 4 ˚C in the dark. To make a comparison, non-biotin DVDMS liposome (DL) was prepared as described above, but DSPE-mPEG 2000 was used as the PEG-lipid instead of DSPE-PEG 2000–biotin.

Liposomes were characterized (i.e., particle size, polydispersity index (PDI), and zeta potential) using a Delsa Nano C Size/Zeta Potential Analysis Instrument (Beckman Instruments, German) at 25 ˚C. The encapsulation efficiencies of DVDMS in liposomes were calculated using the formula EE% = (W_{encap}/W_{total}) × 100%, where W_{encap} is the measured amount of DVDMS in the liposome suspensions after passing over the Sephadex column, and W_{total} is the measured amount of DVDMS in the liposome suspensions before passing over the column. The DVDMS concentration was determined using the fluorescent spectrophotometric method (λ_{ex} = 408 nm, λ_{em} = 626 nm).

2.4.2 *Preparation of biotinylated MBs (MBs-biotin)*

MBs-biotin were prepared as previously described [26]. Briefly, appropriate amounts of DPPC, cholesterol, and DSPE-PEG 2000–biotin (molar ratio of 65:25:10) were added into chloroform. The phospholipid solutions were blended and the solvent was removed through vacuum evaporation under reduced pressure for 2 h. The thin dried phospholipid blends were hydrated at 60 ˚C for 5 min with glycerol-PBS buffer (PBS:glycerol at a volume ratio of 9:1, pH 7.2; 4 mg/mL of final lipid concentration) followed by the addition of perfluoropropane (C_3F_8), and then sealed into a tight vial. The admixture was mechanically vibrated for 120 s to obtain MBs-biotin. Then these MBs were washed thrice with PBS in a bucket rotor and centrifuged at 500*g* for 8 min to remove excess unincorporated lipids. To make a comparison, non-biotin MBs were prepared as described above, but DSPE-mPEG 2000 was used as the PEG-lipid instead of DSPE-PEG 2000–biotin. The MBs were characterized using the Delsa Nano C Size/Zeta Potential Analysis Instrument at 25 ˚C.

2.4.3 *Conjugation of DVDMS liposomes to MBs*

A given amount of avidin (final concentration 0.04 mg/mL) was added into the DL-biotin dispersion. After incubation for 15 min at 25 ˚C. MBs-biotin were added and incubated with liposomes for another 30 min with gentle shaking. The formed DLMB suspension was washed thrice to remove unreacted avidin and free substrate. The DLMBs were characterized using the Delsa Nano C Size/Zeta Potential Analysis Instrument at 25 ˚C. The concentration of DVDMS in the complex was determined using the fluorescent spectrophotometric method.

2.5 Spectral properties assay

To analyze the spectral properties of composited DLMBs, the absorption spectra of DLMBs was recorded in the range from 350 to 750 nm with a resolution of 1 nm, using a multivolume spectrophotometer system (Epoch, BioTek, USA). The fluorescence spectra of DLMBs were also measured with a resolution of 1 nm, using a fluorescence spectrophotometer (LS-55, Perkin Elmer Company, USA). Then, the fluorescence excitation was set at an appropriate wavelength, and the emission spectra of DVDMS with different concentrations were also recorded.

2.6 Observation of the attachment of the liposomes with MBs

2.6.1 *Flow cytometry assay*

To assess the conjugation of liposomes and MBs in DLMBs by flow cytometry, rhodamine-labeled MBs-

biotin (containing 0.5% of rhodamine added into the shell of MBs) were prepared as described above. These labeled MBs-biotin replaced the non-fluorescent MBs-biotin to conjugate with DL-biotin, forming DVDMS liposome (rhodamine-labeled) MBs (DLMBs-rhodamine). The DLMBs-rhodamine were diluted appropriately in PBS buffer, and then detected by flow cytometry (NovoCyte™, ACEA Biosciences Inc., CA, USA), by measuring the fluorescence of DVDMS and rhodamine.

2.6.2 *Laser scanning confocal microscope observation*

The DLMBs-rhodamine suspension was diluted appropriately in PBS buffer and added to a glass-bottom dish (MatTek Corporation, USA). Then, the suspension was morphologically characterized under a laser scanning confocal microscope (LSCM, Model TCS SP5, Leica, Germany) and analyzed by Image-proplus 5.1 software (Media Cybernetics Inc., USA).

2.7 Detection of acoustic cavitation

Terephthalate dosimetry provides a direct sono-chemical efficiency that is sensitive to hydroxyl radicals (·OH). Non-fluorescent terephthalic acid (TA) reacts with ·OH to become fluorescent 2-hysroxyterephthalate ions (HTA); the fluorescence intensity of HTA can be used as acoustic cavitation level indicator. As we previously mentioned [34], the prepared TA solution (1×10^{-4} M) was subjected to US treatment with MBs, DL, or DLMBs in the dark. Immediately after sonication, the fluorescence intensity of HTA (λ_{ex} = 310 nm, λ_{em} = 426 nm) was tested using a fluorescence spectrophotometer.

2.8 Lipid oxidation in DLMBs under US exposure

The lipid oxidation of DLMBs induced by US was detected using the modified ferric thiocyanate (FTC) method, as previously described [35]. Briefly, a MB, DL, or DLMB suspension in a thin-well poly-propylene tube was subjected to US treatment. After 10 min, the samples were diluted in 75% ethanol. An aliquot of 30% ammonium thiocyanate solution and 0.02 M $FeCl_2$ in 3.5% HCl was added to the mixture. After incubation for 10 min, the absorbance at 500 nm was recorded using a SpectraMax M5 Multi-Mode Microplate Reader (Molecular Devices, LLC., CA, USA).

2.9 DVDMS release from DLMBs triggered by US

The release of DVDMS from DLMBs under US exposure was evaluated using the dialysis method. Briefly, a thin-walled polypropylene tube containing DLMBs or DL was placed in the focal zone of the focused US transducer. After US treatment, DLMBs or DL was placed into a dialysis bag (M_W 3,000) within 200 mL dialysis buffer (PBS, pH 7.2) and dialyzed for 3 h to remove free DVDMS. Then, the solution retained in the bag was collected and completely ruptured by Triton X-100. The concentration of DVDMS in either DLMBs or DL was determined using the fluorescent spectrophotometric method. The released DVDMS fraction (%) was calculated using the following formula: RF% = $(1 - F_{son}/F_0) \times 100\%$, where F_0 is the initial fluorescence intensity of DVDMS in a non-treated sample, and F_{son} is the fluorescence intensity of DVDMS in the sonicated sample.

2.10 Detection of cell membrane integrity

MDA-MB-231 cells were seeded at 2×10^5 cells/mL on a 35-mm dish (Corning Inc., Tewksbury, MA, USA) and cultured overnight. To measure the changes of membrane permeability induced by different treatments, an FD 500 uptake assay was performed as previously described [36]. Briefly, DL, free DVDMS, or DLMBs (with the same final concentration of DVDMS = 1 μg/mL) were added into the cultured medium of cells and then sonicated in the presence of FD 500 (1 mg/mL). After US irradiation, the cells were immediately washed thrice with PBS, and the FD 500-positive cells were quantified by flow cytometry.

2.11 Estimating cellular uptake of DVDMS under US exposure

MDA-MB-231 cells were seeded at 2×10^5 cells/mL on 35-mm dishes and cultured overnight. To assess the cellular uptake of DVDMS qualitatively, DLMBs, DL, and free DVDMS (with the same final concentration of DVDMS = 1 μg/mL) were added to the cells and then subjected to US exposure. At 30 min after treatment, the cells were collected and washed thrice with PBS. For each sample, 10,000 cells were analyzed by flow

cytometry, and the mean fluorescence intensity of DVDMS was recorded to represent the uptake of DVDMS in MDA-MB-231 cells.

2.12 Therapeutic treatment protocols

MDA-MB-231 cells in the exponential phase were collected, suspended in culture medium at 2×10^5 cells/mL, and cultured in 35-mm dishes overnight. Then, all samples were randomly divided into control, US, DVDMS alone plus US (abbreviated as free DVDMS), DL plus US (abbreviated as DL), and DLMBs plus US (abbreviated as DLMBs) groups. For the free DVDMS, DL, and DLMBs groups, the DVDMS was at the same concentration of 1 μg/mL. Except the control group, all groups were exposed to US in the presence of a similar number of MBs as that in the DLMBs group (approximately 4×10^6 MBs). For sonication, the cells were exposed to an intensity of 0.4 W/cm^2 with a frequency of 1.0 MHz, duty cycle of 30%, and duration of 90 s.

The tumoral growth and metastatic spread of 4T1 tumors in BALB/c mice very closely mimics stage IV human breast cancer [37]. Therefore, the 4T1 tumor-bearing mouse model is widely used in breast cancer research. In this study, all agents were administered through intratumoral injections with the aid of a stereotaxic instrument (Stoelting, Zenda Inc., Shanghai, China). The tumor-bearing mice were randomly assigned to six groups (with eight mice per group): control (saline injection), free DVDMS (DVDMS concentration at 4 μg/injection), DL (DVDMS concentration at 4 μg/injection), DLMBs 1 (DVDMS concentration at 0.4 μg/injection), DLMBs 2 (DVDMS concentration at 2 μg/injection), and DLMBs 3 (DVDMS concentration at 4 μg/injection). In the free DVDMS and DL groups, the agents were mixed with MBs at equal numbers to those in the DLMBs 3 group. At 10 min after injection, the tumor was placed downward directly at the focal point for sonication with load power of 3 W and frequency of 1.0 MHz for 3 min. The entire procedure (agent administration and sonication) was performed thrice, once every three days.

2.13 *In vitro* cytotoxic analysis

Cell viability was measured by an MTT assay, which was based on the reduction of tetrazolium salt to formazan crystals by living cells. After the different treatments, the cells were harvested and added to 96-well culture plates (100 μL/well), and the viability was determined at 24 h. Briefly, 10 μL MTT solution (5 mg/mL in PBS) was added to each well and the mixture was incubated for an additional 4 h at 37 ℃ in a CO_2 incubator. The formed formazan crystals were dissolved in DMSO and the absorbance at 570 nm was recorded using a microplate reader (ELX800, Bio-Tek, USA). The cell viability of the treated cell samples was then obtained by comparing it to that of the incubated but non-treated control.

A colony formation assay was performed to evaluate the long-term proliferative potential of MDA-MB-231 cells following treatment. Cells were harvested and counted by the trypan blue exclusion test, and then seeded into 24-well plates at 1,000 cells/well and cultured for 7 days. The medium was changed every 3 days until visible colonies formed. Then, the colonies were fixed with formaldehyde for 15 min after being washed with PBS, and then stained with crystal violet for 30 min. Colonies in each group were manually counted, and the cloning efficiency was calculated using the following equation: relative clone formation rate (%) = number of clones in treatment group/number of clones in control group × 100%.

A scanning electron microscope (SEM) is useful to observe cell damage. At 24 h after treatment, the cells were fixed in 2.5% glutaraldehyde, and then washed by PBS, dehydrated by graded alcohol, displaced by isoamyl acetate, dried at the critical point, gold evaporated, and observed under an SEM (S-3400N, Hitachi, Tokyo, Japan).

2.14 Intracellular ROS detection and mitochondrial membrane potential changes

Intracellular ROS production was tested by flow cytometry with DCFH-DA, as previously described [10]. Data are expressed as the percentage of cells with higher fluorescence intensity of DCF among 10,000 cells.

Flow cytometric tests of mitochondrial membrane potential changes of MDA-MB-231 cells were performed using the fluorescent dye rhodamine, as described previously [10]. Data are expressed as the

percentage of cells with lower fluorescence intensity of rhodamine among 10,000 cells.

2.15 Apoptosis evaluation

Quantification of cell apoptosis was performed at 24 h post treatment by Annexin V-FITC/PI double staining, as described previously [34]. Briefly, 100 μL of each sample were suspended in a mixture of working buffer containing Annexin V-FITC and PI. After incubation at 37 ℃ for 30 min, 10,000 cells of each group were analyzed by flow cytometry.

2.16 Distribution of DVDMS and ROS generation detection *in situ*

The effect of DLMBs and US treatment on the intratumoral distribution of DVDMS was examined in 4T1 tumor-bearing BALB/c mice. For autologous control, two xenograft tumors were specifically inoculated on either side of the dorsal subcutaneous part. When the tumor volume reached approximately 5 mm in diameter, the mice were intratumorally injected with DLMBs (DVDMS dose at 2 μg/injection) at the same depth (3 mm), using a stereotaxic instrument. After 10 min, the tumors were subjected to US exposure at 3 W/cm^2 for 3 min. The tumors were collected and frozen sectioned at 10-μm thickness until they measured only 300 μm in thickness, and the fluorescence distribution of DVDMS was observed using a stereo fluorescence microscope (Discovery V20, Zeiss, Germany).

For ROS generation detection *in situ*, the fluorescent probe DCFH-DA (50 μg/injection) was co-injected with DLMBs (2 μg/injection of DVDMS). After 10 min, the tumors were subjected to US exposure at 3 W/cm^2 for 3 min. The tumors were collected, frozen sectioned at 10-μm thickness, stained with DAPI, and observed using a stereoscopic fluorescence microscope.

2.17 *In vivo* sonodynamic anti-tumor effects

After treatment, tumor growth and the body weight of mice were measured every day. Tumor growth was determined by measuring the longest (a) and shortest (b) diameter using a caliper, and the tumor volume (V) was calculated according to the following formula: $V = (a \times b^2)/2$. The mice were sacrificed at the end of experiment. Solid tumors were excised and weighed. A portion of the tumors and main organs (i.e., the heart, liver, spleen, lung, and kidney) were fixed in buffered formalin for histological and immunohistochemical analyses.

For histological examination, tumor tissues and the main organs from different groups were fixed with 10% buffered formalin for 24 h, and then paraffin-embedded, sectioned, and stained with hematoxylin and eosin (H&E). Histopathological changes were observed under a light microscope.

2.18 Terminal deoxynucleotidyl transferase-mediated dUTP nick-end labeling (TUNEL) assay

To identify cell apoptosis of the tumor tissue, paraffin-embedded tumor tissue sections (5 μm) were stained using a TUNEL assay kit (Beyotime Biotechnology, Shanghai, China). Under a fluorescence microscope, the apoptotic cells exhibited green fluorescence after excitation with blue light.

2.19 Immunohistochemistry analysis of proliferating cell nuclear antigen (PCNA)

The expression level of the PCNA reflects the cell proliferation activity [31]. In the present study, the paraffin-embedded tumor tissue sections were dewaxed, rehydrated, and treated with antigen retrieval reagent in 10 mM citrate buffer (pH 6.0) for 15 min in a microwave oven. Sections were immersed in 3% hydrogen peroxide solution for 10 min to quench endogenous peroxidase activity. Non-specific binding was prevented by incubation with 5% normal goat serum for 15 min. The sections were incubated with monoclonal anti-PCNA antibody (Abcam, Cambridge, UK) overnight at 4 ℃. Then, antibody binding was detected using a horseradish peroxidase-conjugated secondary antibody (Zhongshan Golden Bridge Biotechnology Co., Beijing, China) for 1 h at 37 ℃. The sections were visualized with diaminobenzidine (DAB) solution, lightly counterstained with hematoxylin, and observed using light microscopy.

2.20 Statistical analysis

SPSS 19.0 software (SPSS Inc., Chicago, USA) was used for statistical analysis. All data are expressed

as the mean ± standard deviation (S.D.). Differences among the groups were analyzed by one-way ANOVA. A value of $p < 0.05$ was considered significant.

3 Results and discussion

3.1 Preparation and characterization of composite DLMBs

In this study, composite liposome-MBs were synthesized as DVDMS carriers; DVDMS-loaded liposomes were linked onto the MBs' surface via the biotin–avidin linkage (Fig. 1(a)). As shown in Table 1, the diameter of DL was 153.9 ± 13.3 nm, whereas DL-biotin had an average diameter of 150.1 ± 14.6 nm. The size of DVDMS-loaded liposomes (DL and DL-biotin) was slightly larger than that of blank liposomes (135.3 ± 8.9 nm).

Meanwhile, the diameter of biotinylated MBs was 759.0 ± 29.5 nm, and the liposome-loaded MBs were larger (1,009.2 ± 62.8 nm, $p < 0.01$) (Table 1, Fig. 1(b)). The approximately 250-nm increase in the average diameter of the bubbles upon loading with liposomes suggests the formation of a liposome layer on their surface. To better characterize the attachment between the liposomes and MBs, fluorescent rhodamine was used to label the shell of the MBs. Figure 1(c) shows that the DVDMS fluorescence (red) corresponded well with the rhodamine fluorescence (green), indicating that the DVDMS-loaded liposomes were linked onto the MBs validly. Furthermore, we monitored the rate of MBs linking with liposome by quantifying the fluorescence of DVDMS and rhodamine, using flow cytometry. Approximately 67.02% of the MBs that loaded the DVDMS liposomes exhibited high fluorescence intensity Fig. 1(d)). The PDI of various liposome-MB complexes was approximately 0.2, indicating an appropriate size distribution of these particles.

The absorption spectra of DVDMS, DL, and DLMBs are shown in Fig. 2(a). Pure DVDMS (1 μg/mL) exhibited a strong Soret absorption peak at 408 nm, and Q-hands from 500–700 nm. Compared with that of free DVDMS, the spectra of DL and DLMBs presented no changes in the positions and shapes of absorbance bands. Moreover, at the same concentration of DVDMS (1 μg/mL), the fluorescence spectra of DVDMS, DL, and DLMBs showed similar spectral

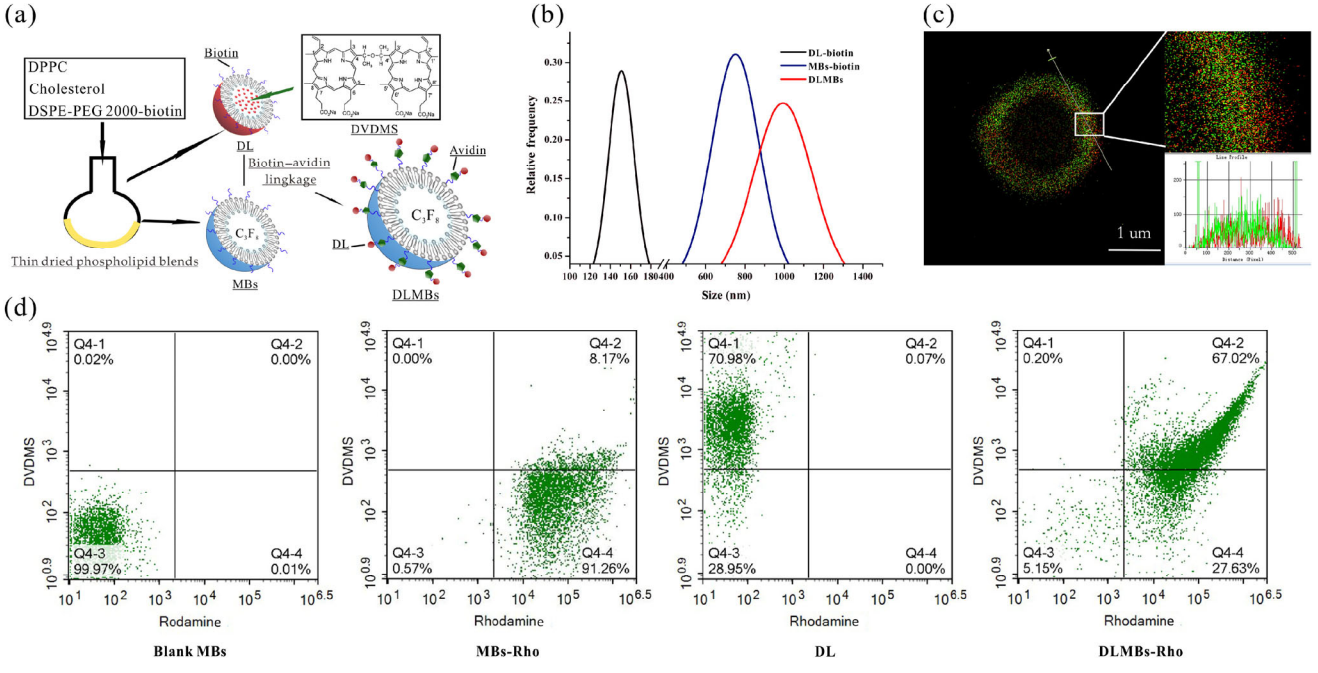

Figure 1 Preparation and characteristics of DLMBs. (a) Schematic of the synthesis process of DLMBs. (b) Hydrodynamic diameters of DL-biotin, MBs-biotin, and DLMBs. (c) Observation of DLMBs by confocal laser scanning microscopy. The profiles on the lower right represent the fluorescence distribution of DVDMS (red) and rhodamine (green) determined as indicated by the white arrow, using Image-proplus 5.1 software. (d) Estimation of MBs linked with DVDMS-loaded liposomes in DLMBs by flow cytometry.

Table 1 Characteristics of DL, MBs, and DLMBs. Data are expressed as mean ± S.D. (n = 150); $^{*}p < 0.05$ versus the blank liposome group; $^{\#\#}p < 0.01$ versus the other groups

Groups	Size (nm)	Zeta potential (mV)	PDI
Blank liposome	135.30 ± 8.90	–37.30 ± 3.01	0.26 ± 0.06
DL	153.90 ± 13.30*	–31.98 ± 1.28	0.21 ± 0.10
DL-biotin	150.10 ± 14.60*	–34.24 ± 4.23	0.24 ± 0.09
Blank MBs	728.40 ± 22.00	–30.81 ± 3.99	0.10 ± 0.03
MBs-biotin	759.00 ± 29.50	–37.64 ± 2.62	0.15 ± 0.07
DLMBs	1,009.20 ± 62.80$^{\#\#}$	–30.95 ± 5.83	0.19 ± 0.11

characteristics (Fig. 2(b); excitation wavelength at 408 nm and emission wavelength at 626 nm). It can be speculated that DVDMS did not change much after being wrapped into the carrier. However, the absorbance values and fluorescence intensities of DL and DLMBs were lower than those of free DVDMS, which may be because DVDMS was encapsulated in the lumen of the liposome and became compressed, resulting in insufficient photon absorption. Moreover, the emission values of DVDMS at 626 nm were dependent on its concentration (Fig. 2(c)). At the range of 0–6.25 μg/mL, the emission values of DVDMS presented a good linear relationship with its concentration, as shown in Fig. 2(d) (the standard linear equation was: $y = 554.4x + 125.6$, $R^2 = 0.9937$). Thus, after lysis, the fluorescence intensity of DVDMS in DL or DLMBs was detected, and its concentration was calculated based on the equation above. The EE% of DVDMS in DL and DL-biotin was 68.73% ± 6.99% and 70.73% ± 3.99% ($p > 0.05$), respectively, suggesting that using biotin-modified phospholipids to assemble the liposomes did not affect the DVDMS loading efficacy, although the size of DL-biotin slightly increased. The DVDMS content of the DLMBs was approximately 40.67% ± 8.43%.

3.2 Release of DVDMS from DLMBs triggered by US

Next, we evaluated the impact of US on the release of DVDMS *in vitro*. DL or DLMBs were exposed to US with various intensities and then dialysed. As shown in Fig. 3(a), the relative release content of the entrapped DVDMS increased significantly with the increase of ultrasonic intensity. When the load power of US was

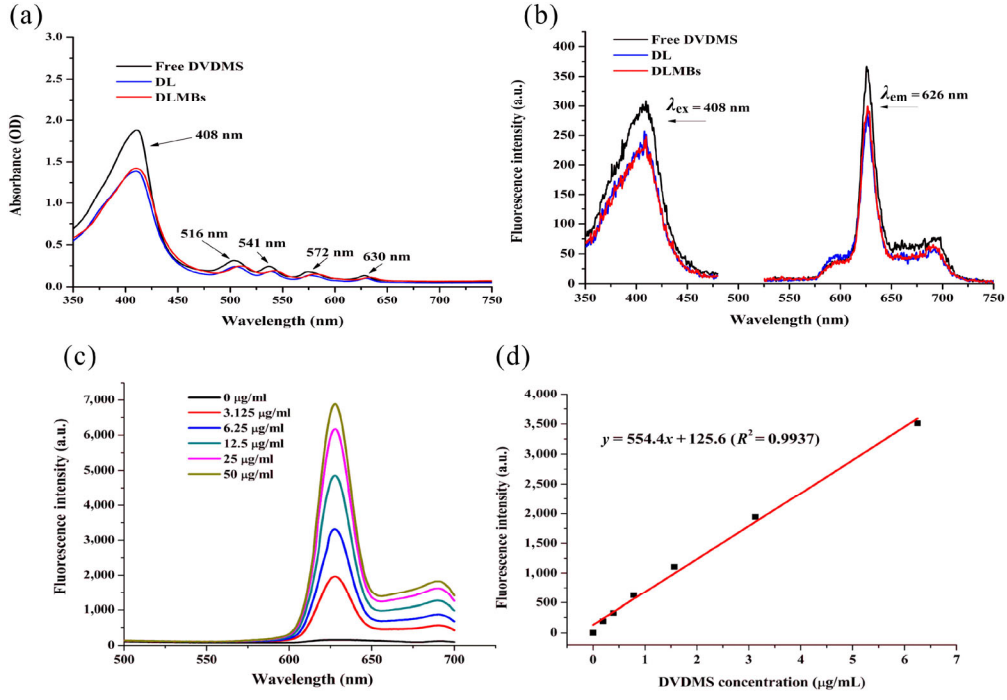

Figure 2 Spectra measurement of DVDMS, DL, and DLMBs. (a) Absorption spectra of DVDMS, DL, and DLMBs at 350–750 nm wavelength. (b) Fluorescence spectra of DVDMS, DL, and DLMBs (350–475 nm for excitation wavelength scanning; 525–750 nm for emission wavelength scanning). (c) Fluorescence emission spectra of DVDMS at different concentrations. (d) Linear dependence of DVDMS fluorescence intensity with its concentration range from 0–6.25 μg/mL measured at 626 nm.

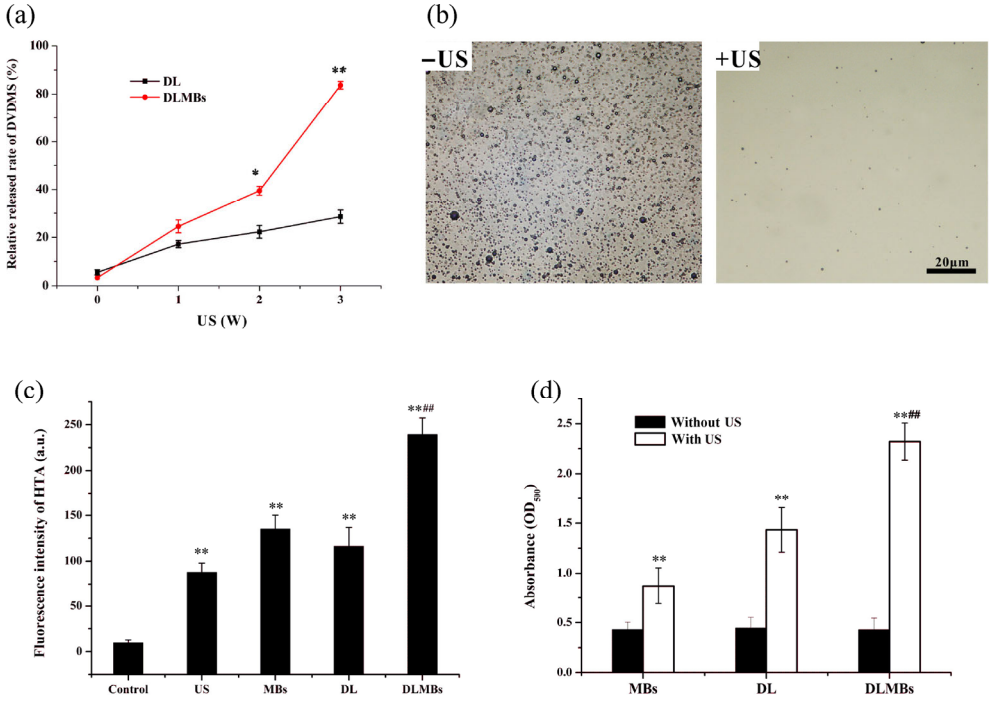

Figure 3 DVDMS release from DLMBs in response to US treatment. (a) Analysis of relative release rate of DVDMS, using the dialysis method. $^{*}p < 0.05$ and $^{**}p < 0.01$ versus the DL group. (b) Optical microscope observation of DLMBs before (left) and after (right) US exposure with load power of 3 W. (c) Evaluation the level of ·OH generation induced by US (load power of 3 W), using the TA method. $^{**}p < 0.01$ versus control; $^{\#\#}p < 0.01$ versus the US, MBs, and DL groups. (d) Evaluation of lipid oxidation caused by US (load power of 3 W), using the FTC assay. $^{**}p < 0.01$ versus the groups without US treatment; $^{\#\#}p < 0.01$ compared with the MBs and DL groups treated by US.

increased up to 3 W, approximately 83.73% ± 3.59% of the DVDMS in DLMBs was released after sonication; whereas, DVDMS in DL without MBs was only released to a certain extent (approximately 28.57% ± 2.77%).

Bright-field microscopy images revealed DLMBs before and after US treatment (Fig. 3(b)). Notably, the bubble-like structure almost disappeared after sonication, suggesting that the integrity of the DLMBs was completely destroyed by US, as reported by other research [38, 39]. In the acoustic field, the change mode of the liposome-MB complex, which is an interesting topic, is still not clear. Emmer et al. suggested that liposome-loaded MBs exhibited "expansion-only" behavior under acoustic pressure when compared with bare MBs. Thus, the presence of liposomes causes a discontinuous change in the shell of MBs [40]. However, McLaughlan et al. proposed that liposome loading had a negligible effect on the destruction threshold for this MB type, and approximately 80% of both populations (bare or liposome-loaded MBs) are destroyed [41]. Although our ultrasonic conditions were slightly different from those in the previous studies, we also observed the same phenomenon, indicating that US could effectively destroy the carrier and trigger the release of DVDMS.

A number of US-triggered release mechanisms for drug-loaded MBs are possible. It seems plausible that the multiple effects of US, including the mechanical shearing action and cavitation effect, all play important roles [19, 20, 24]. One of the aspects to consider is whether the lipid stability of the carrier would be affected by the free radicals induced by acoustic cavitation. In this study, the TA method was applied to measure the ·OH content to assess the level of cavitation. As shown in Fig. 3(c), after US exposure, the ·OH content of the DLMB suspension was much higher than that of the MBs or DL alone, indicating that the combination of DLMBs and US could significantly heighten the level of cavitation. It was speculated that, on the one hand, MBs could reduce the threshold of cavitation and improve the ultrasonic

effects under the acoustic pressure; on the other hand, the released sonosensitizers in the solution are important to enhance cavitation [42]. Phospholipid oxidation caused by free radicals may affect the structural stability of the carrier. Herein, the changes of lipid peroxide were tested by an FTC assay after US treatment. As shown in Fig. 3(d), after sonication with intensity of 3 W, compared with that in the control groups (i.e., the groups of MBs, DL, and DLMBs without US treatment), the concentration of the lipid-oxidized product increased significantly in the US-treated groups. In particular, the oxidized product yield in the DLMBs group was much higher than that in the other groups, which may lead to instantaneous instability of this drug-carrier system and subsequent boosted release of DVDMS.

3.3 Cellular uptake of DVDMS under US plus DLMBs treatment

The results presented in Figs. 4(a) and 4(b) show the effect of US on DVDMS uptake by tumor cells. US could promote the cellular uptake of DVDMS in all groups presented in this study, which is consistent with other relevant Refs. [34, 39, 43]. The enhancement degree of US on DVDMS uptake was much more significant in cells incubated with DLMBs than in the other groups.

Drug-loaded liposomes deliver their therapeutic payload to the targeted cell population through endocytosis; however, the potential mechanism of cellular uptake of drugs under UTMD treatment is much more complicated [20, 44, 45]. According to the report of Meijering et al., endocytosis and pore formation of the plasma membrane are both involved in the process of compound delivery mediated by US and MBs, and the transfer efficiency depends on the molecule size [46]. The increment of the cell membrane permeability induced by sonoporation could be a key factor facilitating the intracellular uptake of DVDMS. As shown in Fig. 4(c), the permeability of the cytoplasm

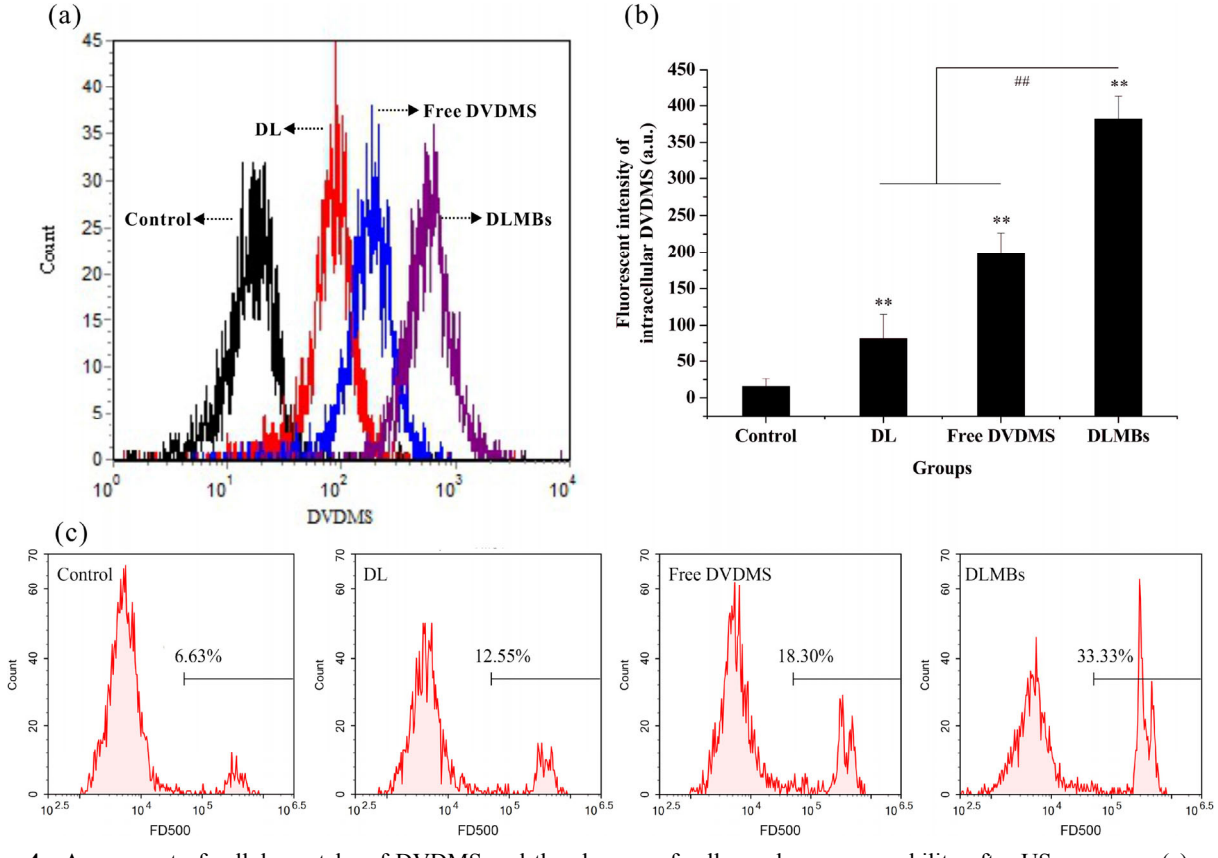

Figure 4 Assessment of cellular uptake of DVDMS and the changes of cell membrane permeability after US exposure. (a) and (b) Quantification of cellular uptake efficiency of DVDMS by flow cytometry. In the histogram (b), $^{**}p < 0.01$ versus control, $^{\#\#}p < 0.01$ versus the DL and free DVDMS groups. (c) Detection of cell membrane permeability, by FD500 staining with flow cytometry.

membrane was clearly affected by DLMBs plus US, based on the FD 500 staining and flow cytometry test results, indicating that US indeed caused obvious sonoporation on MDA-MB-231 cells. Besides the sonoporation, a local high-speed micro-jet caused by cavitation was also considered an important factor because it may increase the movement speed of the drug molecules. Under the comprehensive effects of various factors, the intracellular DVDMS uptake was maximized by US plus DLMBs treatment. Additionally, the cellular content of DVDMS in the DL group was slightly lower than that in the free DVDMS group. We speculated that under *in vitro* experimental condition, free drug molecules may be more likely to transport into cells with the help of US because they is significantly smaller than the liposomal form.

3.4 Sonodynamic cytotoxicity of DLMBs

The cytotoxicity of free DVDMS, DL, or DLMBs alone was observed after incubation with cells for 24 h in the dark; no obvious cytotoxic effects were detected (data not shown). Then, to evaluate the sono-cytotoxicity of the composite DLMBs on breast cancer cells *in vitro*, the MTT assay was performed at 24 h following treatments (Fig. 5(a)). The rate of cell death caused by US alone was less than 10%. Following sonication, approximately 30.43% and 24.93% of cells incubated with free DVDMS and DL, respectively, were killed. Notably, the cell viability decreased to 47.82% in the DLMBs group. A colony formation assay further confirmed that, compared with that of free DVDMS or DL, the long-term proliferation rate of cells was significantly inhibited in the DLMBs group (Figs. 5(b) and 5(c)). Data showed that the cytotoxicity of free DVDMS was slightly higher than that of DL in the presence of US, which may be owing to the difference of intracellular DVDMS uptake between these two groups (Fig. 4).

Meanwhile, the cytotoxic effects were morphologically observed under an SEM. As shown in Fig. 6(a), MDA-MB-231 cells in the control group revealed a typical long spindle shape with an intact membrane and abundant microvilli, with the pseudopodia being at full stretch, tightly sticking to the cover glass. Cells treated with free DVDMS and DL presented some shrinkage, but a relatively regular shape. After DLMB treatment, the cells clearly showed significant morphology changes, more severe shrinkage and roundout, and even collapse. Some papillary protuberances were observed on the cell surface where

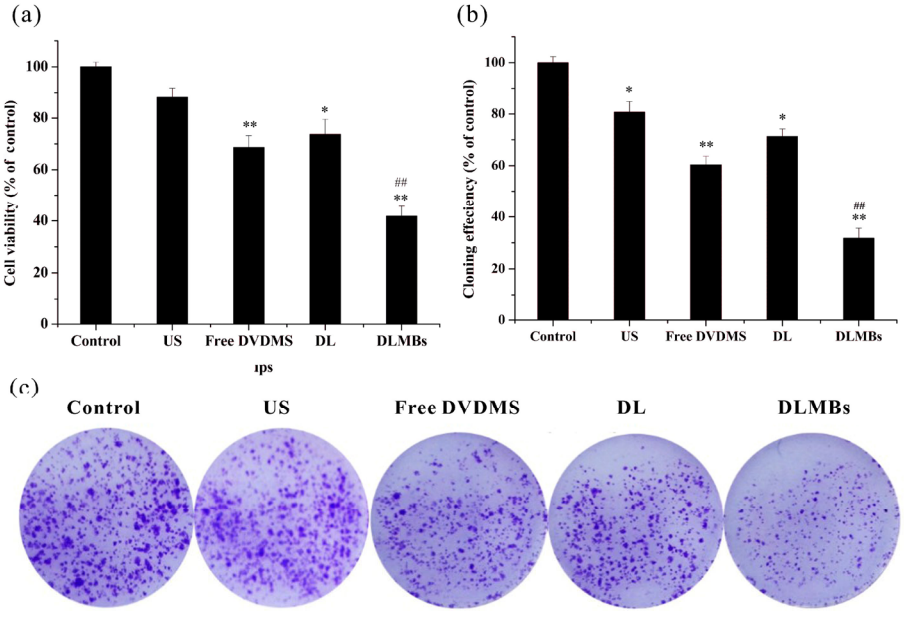

Figure 5 Analysis of sono-cytotoxicity of DLMBs. (a) Cell viability was determined using an MTT assay at 24 h post treatment. (b) and (c) Colony formation assay after different treatments. (b) Quantification of cloning efficiency post treatment. (c) Pictures of cell clone staining with crystal violet. In histograms (a) and (b), $^{*}p < 0.05$ and $^{**}p < 0.01$ versus control, $^{\#\#}p < 0.01$ versus the US, free DVDMS, and DL groups.

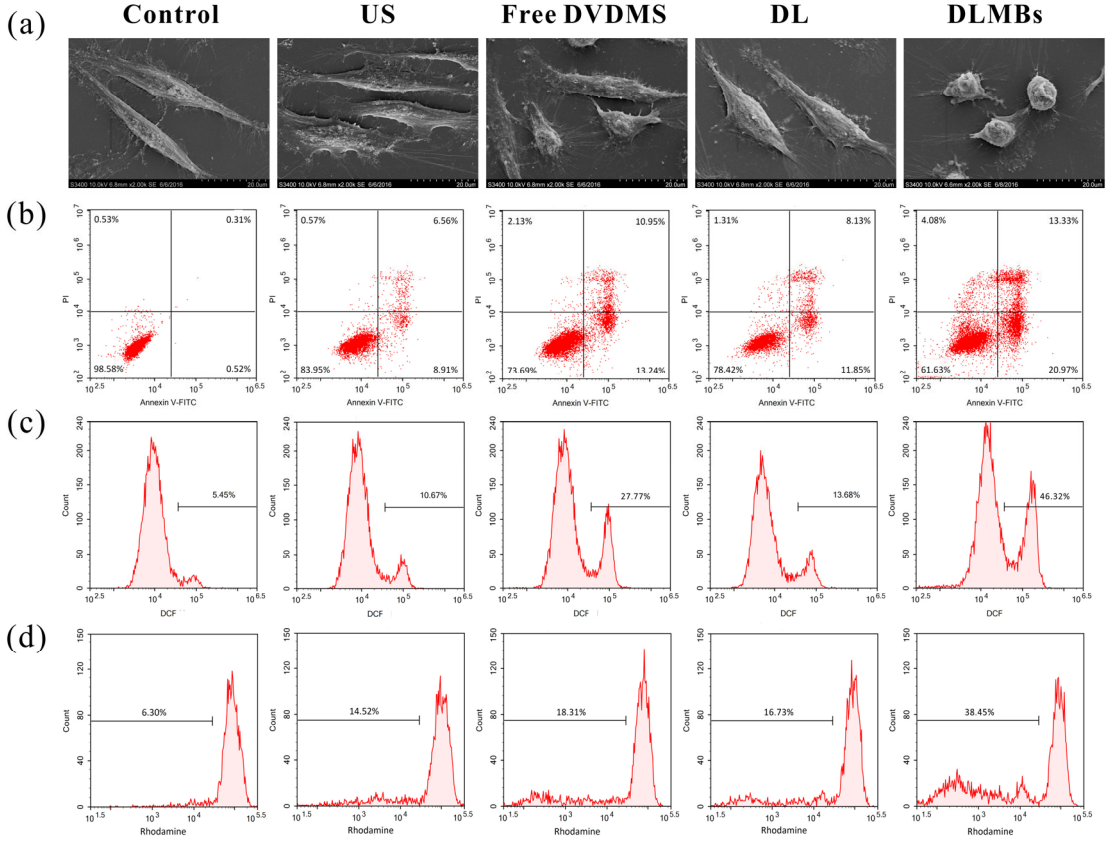

Figure 6 Changes of MDA-MB-231 cells induced by DLMBs plus US *in vitro*. (a) Scanning electron microscopic images of cells after different treatments. Magnification of the images is 2,000×. Scale bars: 20 μm. (b) Apoptosis assessment of MDA-MB-231 cells after different treatments, using Annexin V-FITC/PI staining with flow cytometry. (c) Detection of ROS level using DCFH-DA staining and flow cytometry. (d) Changes of mitochondrial membrane potential were tested by rhodamine staining with flow cytometry.

the cytoplasm seemed to be extruded through the membrane boundary.

Apoptotic cells were analyzed quantitatively by Annexin V-FITC/PI staining with flow cytometry. The results (Fig. 6(b)) demonstrated that DLMBs induced apoptosis at a rate of up to 34.30%, compared with the rate in cells treated with free DVDMS (24.19%) or DL (19.98%), indicating that DLMBs combined with US significantly promoted apoptosis in MDA-MB-231 cells. All these data displayed the remarkable sonocytotoxicity induced by the combinatorial treatment of DLMBs and US.

SDT refers to the synergistic effect of US and sonosensitizers. The proposed mechanisms of SDT-induced cell death mainly focus on the generation of intracellular ROS. Some radical products derived from the sonosensitizer produced during the SDT process, such as singlet oxygen and alkoxy radicals, as well as the reduced antioxidant capacity of tumor cells, all play an important role in the anti-cancer efficacy of SDT [4, 5, 10, 18]. Hence, in our work, intracellular ROS generation of MDA-MB-231 cells was examined by flow cytometry using DCFH-DA staining; DCF green fluorescence indicates adequate cellular ROS levels. Results in Fig. 6(c) showed that under US exposure, free DVDMS caused a content increment of the ROS level (27.77% of cells with high DCF fluorescence), which was slightly higher than that of the DL group (13.68% of cells with high DCF fluorescence). This may be owing to the higher content of cellular DVDMS in cells incubated with free DVDMS (Fig. 4). Notably, DLMBs plus US facilitated ROS generation significantly, with the high DCF green fluorescence cells accounting for 46.32%, showing excellent sonodynamic effect.

In our previous work, we found that DVDMS was mainly distributed in the mitochondria of tumor cells, with DVDMS-mediated SDT resulting in serious

mitochondrial dysfunction [14, 32, 33, 47]. To investigate whether mitochondria were damaged in MDA-MB-231 cells, rhodamine was used to measure the change of mitochondrial membrane potential. The data obtained from flow cytometry (Fig. 6(d)) confirmed that after being treated with DLMBs plus US, the number of cells with lower fluorescence intensity of rhodamine significantly increased. The influence of SDT on mitochondria is complicated. Studies have confirmed that the site of sonosensitizer localization is potentially important for cancer therapy, because of the very short lifetime and diffusion distance of some radical products derived from the sonosensitizer produced during the SDT process. Mitochondria are also the main source of ROS generation, as well as one target attacked by ROS. Based on the data above, it was speculated that mitochondria were affected in close relation with ROS generation, which contributed to the cell death induced by DLMBs plus US treatment.

3.5 Intratumoral diffusion of DVDMS and ROS generation affected by DLMBs and US

Numerous investigations have shown that US can promote the accumulation of drugs in tumors with high or low enhanced permeation and retention (EPR) levels [48]. Besides, the efficiency of US on drug delivery is much greater with the help of targeted factors (such as folate, transferrin, and arginyl-glycyl-aspartic acid (RGD) tripeptide) [49]. In the present study, the distribution of sonosensitizers within tumor tissues under US exposure was highlighted. DLMBs were successfully injected into the tumor tissue *in situ* in the same depth and then sonicated. Then, DVDMS fluorescence of a frozen section of the tumor tissue was observed using a stereo fluorescence microscope. As shown in Fig. 7, the red fluorescence of DVDMS diffused throughout the tumor section after US treatment, whereas the fluorescence was just gathered brightly in the untreated group, suggesting that the combination of DLMBs with US could promote the intratumoral diffusion of DVDMS.

On the basis of these results, ROS might play a vital role not only in the boosted release of DVDMS from DLMBs triggered by US but also in the process of sono-cytotoxicity mediated by DLMBs and US. Herein, we simultaneously tested the ROS generation for the duration of the DLMBs plus US treatment. Interestingly, Fig. 8 shows that the ROS-related green fluorescence of DCF was diffused extensively in the treated tumor section where the area showed DVDMS distribution (red fluorescence), whereas negligible DCF fluorescence was detected in the tumor section without US exposure, indicating that significant ROS generation was specific to the DLMBs plus US treatment. Presumably, under US exposure, ROS generation may contribute to promote intratumoral diffusion of DVDMS and enhance its SDT effect *in vivo*.

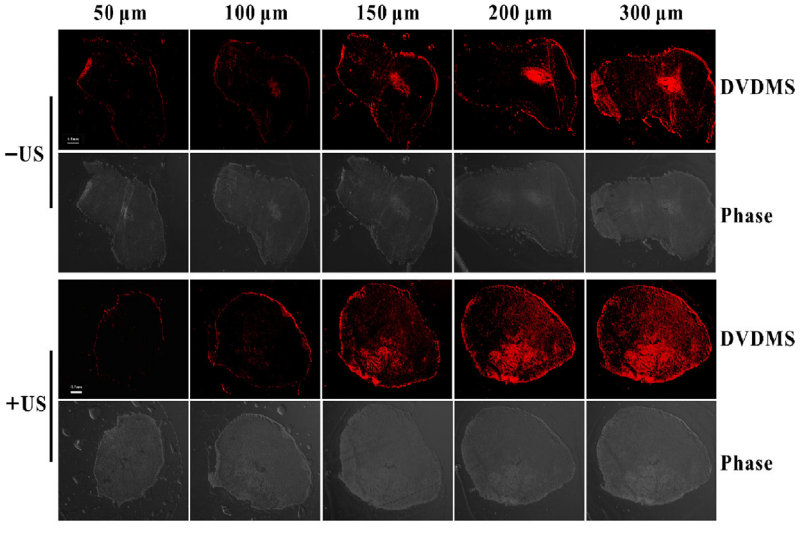

Figure 7 Fluorescent observation of intratumoral distribution of DVDMS after DLMBs with/without US treatment. The corresponding phase contrast images were also captured.

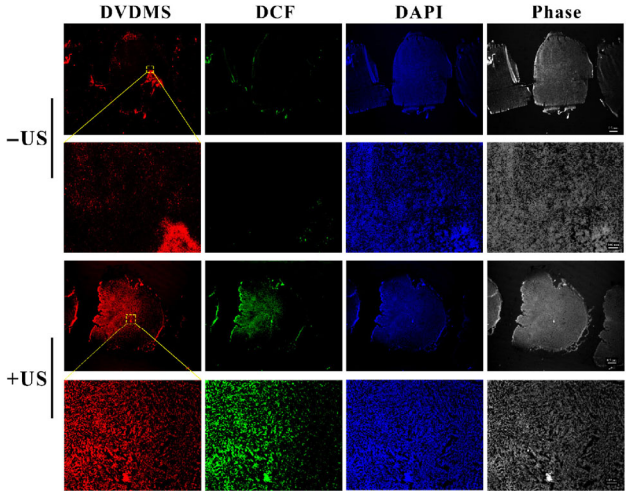

Figure 8 *In vivo* ROS generation observation, using DCFH-DA staining with fluorescence microscopy, after DLMBs with/without US treatment.

3.6 *In vivo* combinatory anti-tumor efficacy of DLMBs with US

To investigate the sonodynamic anti-tumor efficacy of composite DLMBs with US, a 4T1 mouse mammary tumor model was utilized. Tumor-bearing mice were divided into six experimental groups, and the results are shown in Fig. 9. Representative mice were also photographed 14 days after treatments. Both free DVDMS and DL with US inhibited tumor growth (volume and weight) to a certain extent; the tumor weight inhibition ratios were approximately 34.36% and 30.19%, respectively ($p < 0.05$ versus control). Importantly, for the groups treated with DLMBs plus US, tumor growth was greatly retarded with increased dosage; the tumor weight inhibition ratio in the DLMBs 3 group was up to 67.93%, indicating a greater SDT effect against breast cancer. H&E staining revealed obvious tissue damage caused by DLMBs plus US (Fig. 9(d)). The results of TUNEL staining implied that DLMBs caused notable apoptosis of the tumor cells under US exposure (Fig. 10(a)). Moreover, the immunohistochemistry analysis for evaluating the expression level of PCNA—a representative marker of proliferation—showed that PCNA greatly decreased in the DLMBs groups, compared with that in the other groups (Fig. 10(b)). Simultaneously, the body weight of tumor-bearing mice was measured during the experiment, and no major changes were observed following the various treatments (Fig. 11(a)). Histological

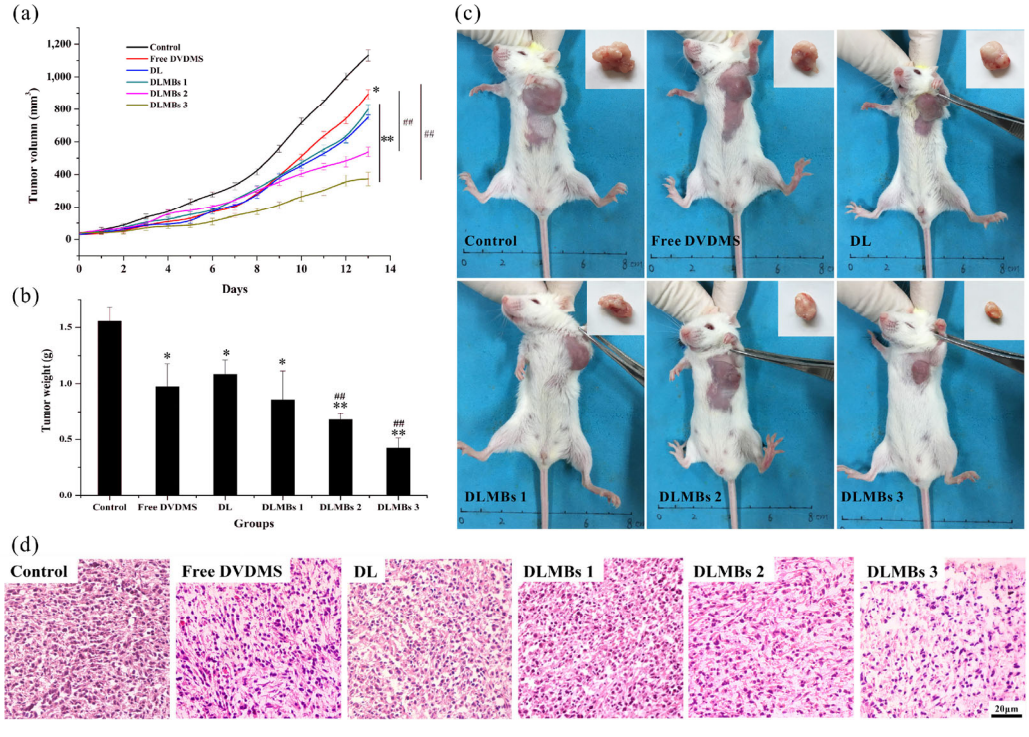

Figure 9 *In vivo* tumor growth inhibition assessment. The average volume (a) and weight (b) of 4T1 tumors are shown. $^{*}p < 0.05$ and $^{**}p < 0.01$ versus control, $^{\#\#}p < 0.01$ versus the free DVDMS and DL groups. (c) Images of representative tumors excised and mice from each group at 14 days after treatment. (d) H&E staining revealed the damage of tumor tissues in each group.

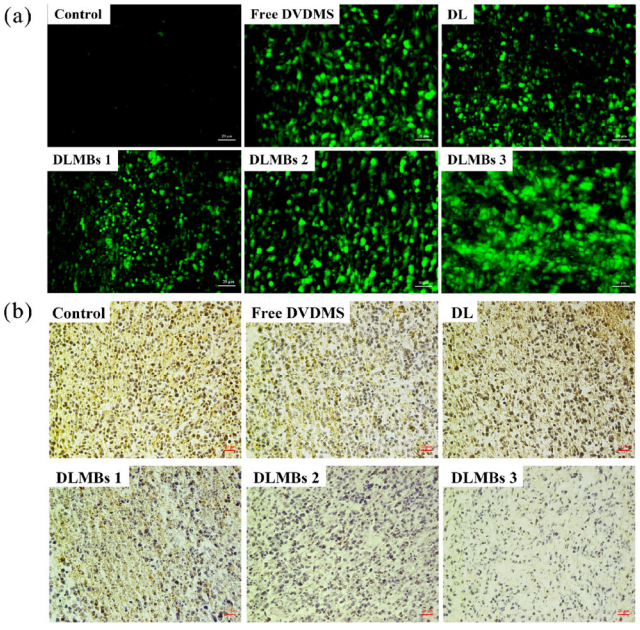

Figure 10 Assessment of tumor cell apoptosis and proliferation activity post treatment *in situ*. (a) Apoptosis determination by the TUNEL assay *in situ*. (b) Immunohistochemistry detection for PCNA.

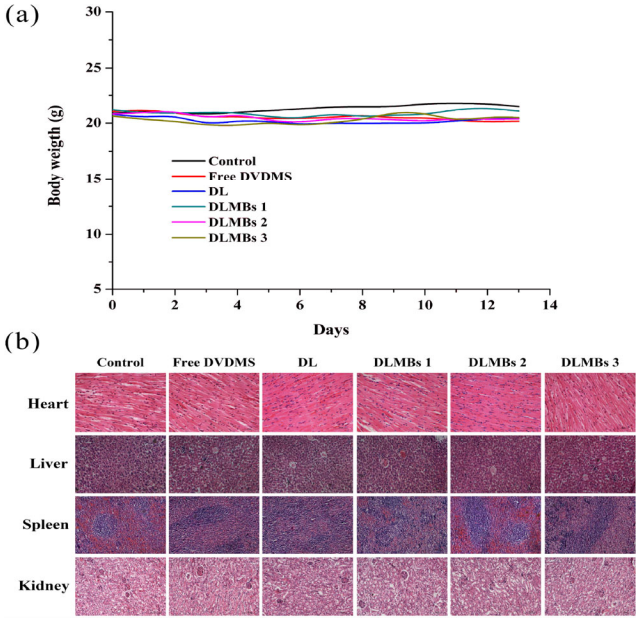

Figure 11 Evaluation of side effects after therapeutic treatment. (a) Plot of mouse body weight versus the number of days post the different treatments. (b) Effect of the different treatments on the structural changes of the major organs (heart, liver, spleen, and kidney) in 4T1-bearing mice, visualized by H&E staining and observed under an optical microscope.

examination of the major organs (i.e., the heart, liver, spleen, and kidney) presented negligible organ damage, indicating good biosafety (Fig. 11(b)).

From these results, the work presented here supported the idea that coupling of DVDMS-loaded liposomes and MBs had good US-responsive activity, and this complex showed better sono-cytotoxicity against breast cancer compared with that of free or liposomal DVDMS. Nevertheless, this study has some limitations. We only performed intratumoral injections to administer the DLMBs to the tumor-bearing mice and assessed its anti-tumor effects combined with US. Our results have confirmed that DLMBs respond well to US, enhancing the SDT effects of DVDMS. However, from a practical perspective, the biodistribution and pharmacokinetics of DLMBs via tail-vein injection still need to be studied. In addition, future studies should examine whether DLMBs can be used as a theranostic platform to enhance US imaging and the sono-cytotoxicity of DVDMS on tumor tissues. Finally, in future research, we will explore whether the sonodynamic therapeutic potential of DLMBs is further improved by functionalizing with a targeting ligand.

4 Conclusions

In conclusion, we synthesized a US-responsive carrier system to carry the new sonosensitizer DVDMS. Both *in vivo* and *in vitro* studies confirmed that DLMBs plus US treatment possesses significant anticancer activity, including apoptosis induction and proliferation inhibition, with minimal side effects. Under DLMBs plus US treatment, the generated ROS may play a vital role to boost DVDMS release from DLMBs, promote its cellular uptake and intratumoral diffusion, and contribute to enhancing the sono-cytotoxicity of DVDMS. The combined treatment caused obvious changes to cell morphology, mitochondrial damage, and cell apoptosis. Histologically, the inhibition of tumor growth appeared to result from increased apoptosis and reduced proliferation activity in mice 4T1 tumors. The US-responsive carrier reported in this study might provide novel insight for the combination of US-mediated sonosensitizer delivery with SDT to achieve better antineoplastic effects.

Acknowledgements

This research was supported by the National Natural

Science Foundation of China (Nos. 81472846 and 81571834), the China Postdoctoral Science Foundation (No. 2016M600684), the Fundamental Research Funds for the Central Universities (No. GK201602003), and the Natural Science Foundation of Shaanxi Province (No. 2017JM8004).

References

[1] Wood, A. K. W.; Sehgal, C. M. A review of low-intensity ultrasound for cancer therapy. *Ultrasound Med. Biol.* **2015**, *41*, 905–928.

[2] Antonelli, A.; Sfara, C.; Magnani, M. Intravascular contrast agents in diagnostic applications: Use of red blood cells to improve the lifespan and efficacy of blood pool contrast agents. *Nano Res.* **2017**, *10*, 731–766.

[3] Di, J.; Yu, J. C.; Wang, Q.; Yao S. S.; Suo, D. J.; Ye, Y. Q.; Pless, M.; Zhu, Y.; Jing, Y.; Gu, Z. Ultrasound-triggered noninvasive regulation of blood glucose levels using microgels integrated with insulin nanocapsules. *Nano Res.* **2017**, *10*, 1393–1402.

[4] McHale, A. P.; Callan, J. F.; Nomikou, N.; Fowley, C.; Callan, B. Sonodynamic therapy: Concept, mechanism and application to cancer treatment. In *Therapeutic Ultrasound*; Escoffre, J. M.; Bouakaz, A., Eds.; Springer International Publishing: Switzerland, 2016; pp 429–450.

[5] Trendowski, M. The promise of sonodynamic therapy. *Cancer Metastasis Rev.* **2014**, *33*, 143–160.

[6] Lv, Y. H.; Zheng, J. H.; Zhou, Q.; Jia, L. M.; Wang, C. Y.; Liu, N. A.; Zhao, H.; Ji, H.; Li, B. X.; Cao, W. W. Antiproliferative and apoptosis-inducing effect of exo-protoporphyrin IX based sonodynamic therapy on human oral squamous cell carcinoma. *Sci. Rep.* **2017**, *7*, 40967.

[7] Sun, H. Z.; Ge, W. J; Gao, X.; Wang, S. S.; Jiang, S. J.; Hu, Y.; Yu, M.; Hu, S. S. Apoptosis-promoting effects of hematoporphyrin monomethyl ether-sonodynamic therapy (HMME-SDT) on endometrial cancer. *PLoS One* **2015**, *10*, e0137980.

[8] Inui, T.; Amitani, H.; Kubo, K.; Kuchiike, D.; Uto, Y.; Nishikata, T.; Mette, M. Case report: A non-small cell lung cancer patient treated with GcMAF, sonodynamic therapy and tumor treating fields. *Anticancer Res.* **2016**, *36*, 3767–3770.

[9] Jia, Y. L.; Wang, X. B.; Liu, Q. H.; Leung, A. W.; Wang, P.; Xu, C. S. Sonodynamic action of hypocrellin B triggers cell apoptoisis of breast cancer cells involving caspase pathway. *Ultrasonics* **2017**, *73*, 154–161.

[10] Li, Y. X.; Wang, P.; Wang, X. B.; Su, X. M.; Liu, Q. H. Involvement of mitochondrial and reactive oxygen species in the sonodynamic toxicity of chlorin e6 in human leukemia K562 cells. *Ultrasound Med. Biol.* **2014**, *40*, 990–1000.

[11] Wang, X. J.; Mitchell, D.; Lewis, T. J. Primary clinical use of sonodynamic therapy (SDT) for advanced breast cancer. *J. Clin. Oncol.* **2008**, *26*, 12029.

[12] Huang, P.; Qian, X. Q.; Chen, Y.; Yu, L. D.; Lin, H.; Wang, L. Y.; Zhu, Y. F.; Shi, J. L. Metalloporphyrin-encapsulated biodegradable nanosystems for highly efficient magnetic resonance imaging-guided sonodynamic cancer therapy. *J. Am. Chem. Soc.* **2017**, *139*, 1275–1284.

[13] Deepagan, V. G.; You, D. G.; Um, W.; Ko, H.; Kwon, S.; Choi, K. Y.; Yi, G. R.; Lee, J. Y.; Lee, D. S.; Kim, K. et al. Long-circulating Au-TiO_2 nanocomposite as a sonosensitizer for ROS-mediated eradication of cancer. *Nano Lett.* **2016**, *16*, 6257–6264.

[14] Wang, H. P.; Wang, P.; Li, L.; Zhang, K.; Wang, X. B.; Liu, Q. H. Microbubbles enhance the antitumor effects of sinoporphyrin sodium mediated sonodynamic therapy both *in vitro* and *in vivo*. *Int. J. Biol. Sci.* **2015**, *11*, 1401–1409.

[15] McEwan, C.; Kamila, S.; Owen, J.; Nesbitt, H.; Callan, B.; Borden, M.; Nomikou, N.; Hamoudi, R. A.; Taylor, M. A.; Stride, E. et al. Combined sonodynamic and antimetabolite therapy for the improved treatment of pancreatic cancer using oxygen loaded microbubbles as a delivery vehicle. *Biomaterials* **2016**, *80*, 20–32.

[16] McEwan, C.; Fowley, C.; Nomikou, N.; McCaughan, B.; McHale, A. P.; Callan, J. F. Polymeric microbubbles as delivery vehicles for sensitizers in sonodynamic therapy. *Langmuir* **2014**, *30*, 14926–14930.

[17] Chen, H.; Hwang, J. H. Ultrasound-targeted microbubble destruction for chemotherapeutic drug delivery to solid tumors. *J. Ther. Ultrasound* **2013**, *1*, 10.

[18] Fu, Z. W.; Popov, V. Parametric study of acoustically-driven microbubble cavitations in a sonochemical reactor. *Ultrason. Sonochem.* **2014**, *21*, 415–427.

[19] Yoon, Y. I.; Kwon, Y. S.; Cho, H. S.; Heo, S. H.; Park, K. S.; Park, S. G.; Lee, S. H.; Hwang, S. I.; Kim, Y. I.; Jae, H. J. et al. Ultrasound-mediated gene and drug delivery using a microbubble-liposome particle system. *Theranostics* **2014**, *4*, 1133–1144.

[20] Ibsen, S.; Schutt, C. E.; Esener, S. Microbubble-mediated ultrasound therapy: A review of its potential in cancer treatment. *Drug Des. Devel. Ther.* **2013**, *7*, 375–388.

[21] Wang, Q. X.; Manmi, K.; Liu, K. K. Cell mechanics in biomedical cavitation. *Interface Focus* **2015**, *5*, 20150018.

[22] Zhang, L.; Sun, Z. X.; Ren, P. P.; You, M. J.; Zhang, J.; Fang, L. Y.; Wang, J.; Chen, Y. H.; Yan, F.; Zheng, H. R. et al. Localized delivery of shRNA against PHD2 protects

the heart from acute myocardial infarction through ultrasound-targeted cationic microbubble destruction. *Theranostics* **2017**, *7*, 51–66.

[23] Dewitte, H.; Vanderperren, K.; Haers, H.; Stock, E.; Duchateau, L.; Hesta, M.; Saunders, J. H.; De Smedt, S. C.; Lentacker, I. Theranostic mRNA-loaded microbubbles in the lymphatics of dogs: Implications for drug delivery. *Theranostics* **2015**, *5*, 97–109.

[24] Kheirolomoom, A.; Dayton, P. A.; Lum, A. F. H.; Little, E.; Paoli, E. E.; Zheng, H. R.; Ferrara, K. W. Acoustically-active microbubbles conjugated to liposomes: Characterization of a proposed drug delivery vehicle. *J. Control. Release* **2007**, *118*, 275–284.

[25] Geers, B.; Lentacker, I.; Sanders, N. N.; Demeester, J.; Meairs, S.; De Smedt, S. C. Self-assembled liposome-loaded microbubbles: The missing link for safe and efficient ultrasound triggered drug-delivery. *J. Control. Release* **2011**, *152*, 249–256.

[26] Deng, Z. T.; Yan, F.; Jin, Q. F.; Li, F.; Wu, J. R.; Liu, X.; Zheng, H. R. Reversal of multidrug resistance phenotype in human breast cancer cells using doxorubicin-liposome-microbubble complexes assisted by ultrasound. *J. Control. Release* **2014**, *174*, 109–116.

[27] Zhu, X.; Guo, J.; He, C. C.; Geng, H. X.; Yu, G. S.; Li, J. Q.; Zheng, H. R.; Ji, X. J.; Yan, F. Ultrasound triggered image-guided drug delivery to inhibit vascular reconstruction via paclitaxel-loaded microbubbles. *Sci. Rep.* **2016**, *6*, 21683.

[28] Fang, Q.; Yang, D. A porphyrin dimer salt combined with the ether bond and its manufacturing method. China Patent ZL200910179116.5, Aug 29, 2012.

[29] Wang, X. B.; Hu, J. M.; Wang, P.; Zhang, S. L.; Liu, Y. C.; Xiong, W. L.; Liu, Q. H. Analysis of the *in vivo* and *in vitro* effects of photodynamic therapy on breast cancer by using a sensitizer, sinoporphyrin sodium. *Theranostics* **2015**, *5*, 772–786.

[30] Yan, X. F.; Hu, H.; Lin, J.; Jin, A. J.; Niu, G.; Zhang, S. L.; Huang, P.; Shen, B. Z.; Chen, X. Y. Optical and photoacoustic dual-modality imaging guided synergistic photodynamic/photothermal therapies. *Nanoscale* **2015**, *7*, 2520–2526.

[31] Yan, X. F.; Niu, G.; Lin, J.; Jin, A. J.; Hu, H.; Tang, Y. X.; Zhang, Y. J.; Wu, A. G.; Lu, J.; Zhang, S. L. et al. Enhanced fluorescence imaging guided photodynamic therapy of sinoporphyrin sodium loaded graphene oxide. *Biomaterials* **2015**, *42*, 94–102.

[32] Xiong, W. L.; Wang, P.; Hu, J. M.; Jia, Y. L.; Wu, L. J.; Chen, X. Y.; Liu, Q. H.; Wang, X. B. A new sensitizer DVDMS combined with multiple focused ultrasound treatments: An effective antitumor strategy. *Sci. Rep.* **2015**, *5*, 17485.

[33] Li, C. F.; Zhang, K.; Wang, P.; Hu, J. M.; Liu, Q. H.; Wang, X. B. Sonodynamic antitumor effect of a novel sonosensitizer on S180 solid tumor. *Biopharm. Drug Dispos.* **2014**, *35*, 50–59.

[34] Li, Y. X.; Wang, P.; Chen, X. Y.; Hu, J. M.; Liu, Y. C.; Wang, X. B.; Liu, Q. H. Activation of microbubbles by low-intensity pulsed ultrasound enhances the cytotoxicity of curcumin involving apoptosis induction and cell motility inhibition in human breast cancer MDA-MB-231 cells. *Ultrason. Sonochem.* **2016**, *33*, 26–36.

[35] Mihaljević, B.; Katušin-Ražem, B.; Ražem, D. The reevaluation of the ferric thiocyanate assay for lipid hydroperoxides with special considerations of the mechanistic aspects of the response. *Free Radic. Biol. Med.* **1996**, *21*, 53–63.

[36] Jia, Y. L.; Yuan, W. J.; Zhang, K.; Wang, J.; Wang, P.; Liu, Q. H.; Wang, X. B. Comparison of cell membrane damage induced by the therapeutic ultrasound on human breast cancer MCF-7 and MCF-7/ADR cells. *Ultrason. Sonochem.* **2015**, *26*, 128–135.

[37] Pulaski, B. A.; Terman, D. S.; Khan, S.; Muller, E.; Ostrand-Rosenberg, S. Cooperativity of *Staphylococcal aureus* enterotoxin B superantigen, major histocompatibility complex class II, and CD80 for immunotherapy of advanced spontaneous metastases in a clinically relevant postoperative mouse breast cancer model. *Cancer Res.* **2000**, *60*, 2710–2715.

[38] Lentacker, I.; Geers, B.; Demeester, J.; De Smedt, S. C.; Sanders, N. N. Design and evaluation of doxorubicin-containing microbubbles for ultrasound-triggered doxorubicin delivery: Cytotoxicity and mechanisms involved. *Mol. Ther.* **2010**, *18*, 101–108.

[39] Yan, F.; Li, L.; Deng, Z. T.; Jin, Q. F.; Chen, J. J.; Yang, W.; Yeh, C. K.; Wu, J. R.; Shandas, R.; Liu, X. et al. Paclitaxel-liposome–microbubble complexes as ultrasound-triggered therapeutic drug delivery carriers. *J. Control. Release* **2013**, *166*, 246–255.

[40] Emmer, M.; van Wamel, A.; Goertz, D. E.; de Jong, N. The onset of microbubble vibration. *Ultrasound Med. Biol.* **2007**, *33*, 941–949.

[41] McLaughlan, J. R.; Harput, S.; Abou-Saleh, R. H.; Peyman, S. A.; Evans, S.; Freear, S. Characterisation of liposome-loaded microbubble populations for subharmonic imaging. *Ultrasound Med. Biol.* **2017**, *43*, 346–356.

[42] Wang, P.; Wang, X. B.; Zhang, K.; Gao, K. L.; Song, M.; Liu, Q. H. The spectroscopy analyses of PpIX by ultrasound irradiation and its sonotoxicity *in vitro*. *Ultrasonics* **2013**, *53*, 935–942.

[43] Yang, S.; Wang, P.; Wang, X. B.; Su, X. M.; Liu, Q. H. Activation of microbubbles by low-level therapeutic ultrasound

enhances the antitumor effects of doxorubicin. *Eur. Radiol.* **2014**, *24*, 2739–2753.

[44] Sennoga, C. A.; Kanbar, E.; Auboire, L.; Dujardin, P. A.; Fouan, D.; Escoffre, J. M.; Bouakaz, A. Microbubble-mediated ultrasound drug-delivery and therapeutic monitoring. *Expert Opin. Drug Deliv.* **2016**, *11*, 1–13.

[45] Qin, J. L.; Wang, T. Y.; Willmann, J. K. Sonoporation: Applications for cancer therapy. In *Therapeutic Ultrasound*; Escoffre, J. M.; Bouakaz, A., Eds.; Springer International Publishing: Switzerland, 2016; pp 263–291.

[46] Meijering, B. D. M.; Juffermans, L. J. M.; van Wamel, A.; Henning, R. H.; Zuhorn, I. S.; Emmer, M.; Versteilen, A. M. G.; Paulus, V. W. J.; van Gilst, W. H.; Kooiman, K. et al. Ultrasound and microbubble-targeted delivery of macromolecules is regulated by induction of endocytosis and pore formation. *Circ. Res.* **2009**, *104*, 679–687.

[47] Wang, H. P.; Wang, X. B.; Zhang, S. L.; Wang, P.; Zhang, K.; Liu, Q. H. Sinoporphyrin sodium, a novel sensitizer, triggers mitochondrial-dependent apoptosis in ECA-109 cells via production of reactive oxygen species. *Int. J. Nanomedicine* **2014**, *9*, 3077–3090.

[48] Theek, B.; Baues, M.; Ojha, T.; Möckel, D.; Veettil, S. K.; Steitz, J.; van Bloois, L.; Storm, G.; Kiessling, F.; Lammers, T. Sonoporation enhances liposome accumulation and penetration in tumors with low EPR. *J. Control. Release* **2016**, *231*, 77–85.

[49] Luo, T. T.; Sun, J. C.; Zhu, S. Y.; He, J.; Hao, L.; Xiao, L. L.; Zhu, Y.; Wang, Q. Q.; Pan, X.; Wang, Z. G. et al. Ultrasound-mediated destruction of oxygen and paclitaxel loaded dual-targeting microbubbles for intraperitoneal treatment of ovarian cancer xenografts. *Cancer Lett.* **2017**, *391*, 1–11.